Dalton Transactions

PAPER

View Article Online
View Journal | View Issue

Cite this: *Dalton Trans.*, 2014, **43**, 16872

Received 19th March 2014,
Accepted 24th August 2014

DOI: 10.1039/c4dt00823e

www.rsc.org/dalton

Mitochondria-targeting phosphorescent iridium(III) complexes for living cell imaging†

Qingqing Zhang,‡[a,b,c] Rui Cao,‡[a,b] Hao Fei[a] and Ming Zhou*[a,d]

Two phosphorescent iridium(III) complexes conjugated to a lipophilic triphenylphosphonium cation moiety, **IrMitoOlivine** and **IrMitoNIR**, were synthesized. The complexes show high mitochondria-specificity and relatively lower cytotoxicity. Time-lapse confocal imaging indicates that both complexes exhibit an excellent anti-photobleaching capability under continuous laser irradiation.

Introduction

Mitochondria are the primary intracellular bioenergy-producing compartments in eukaryotic cells, and are involved in numerous vital cellular processes, such as oxidative stress[1] and apoptosis.[2] The larger membrane potential of *ca.* 180 mV (negative inside) across the mitochondrial membrane[3] compared with other intracellular compartments results in stronger and selective accumulation and retention of cations[4] inside mitochondria. In contrast to polar cations, which require protein carriers to pass through the lipid bilayer, lipophilic cations can actively and easily penetrate the mitochondrial membrane and accumulate inside it,[3a,4] for example, rosamines[5] and carbocyanines.[6] Other than both, a lipophilic triphenylphosphonium (TPP) cation is nonfluorescent but enables delivery of wide varieties of bioactive molecules,[3b,7] such as antioxidants,[8] drugs,[9] and biomacromolecules,[10] into mitochondria. Radioactive isotope labeled TPP cations were reported as positron emission tomography agents in myocardial and tumor imaging.[11] A lot of organic fluorescent probes linked to TPP cations were applied in mitochondria-targeting functional cellular imaging, for example, zinc ions[12] and hydrogen peroxide.[13]

Phosphorescent cyclometalated iridium(III) complexes generally have high quantum efficiencies, large Stokes' shifts, fine emission tunability and excellent anti-photobleachability[14] and thus attract extensive interest in chemosensing[15] and bioimaging.[16] Moreover, the phosphorescence properties of iridium(III) complexes depend on their primary ligands and are able to vary to certain degrees with their ancillary ligands. Combining a phosphorescent iridium(III) complex with a lipophilic TPP cation is a facile way of building up a mitochondria-specific phosphorescent probe[17] while retaining the luminescence properties of the iridium(III) complex herein. Such a probe was first reported by Murase *et al.*[18] However, the first reported TPP functionalized iridium(III) complex probe has an acetylacetonato ancillary, which is a labile ligand and can be replaced by coordinating solvent molecules including water under the attack of protons.[19] Reported in this work are two TPP functionalized iridium(III) complexes with a stable diimine ancillary ligand (Scheme 1). The change of acetylacetonato into a 2,2′-bipyridine derivative leads to a change from the electronically neutral state to the electronically positive state of the iridium(III) phosphores. Thus, in addition to avoiding proton induced degradation, the positively charged phosphores may have extra advantages over the neutral ones, such as better permeability into cells and accessibility to molecular modification. Such cationic phosphorescent iridium(III) complexes have found use in cell imaging.[14b,16a,20]

Results and discussion

Design and synthesis

Two biscyclometalated diimine iridium(III) complexes, the yellowish green emitting bis(2-phenylbenzothiazolato)-(4-methyl-4′-carboxypropyl-2,2′-bipyridine)iridium(III) ([Ir(bt)$_2$]$_2$-(bpy-COOH))[21] and the near infrared (NIR) emitting bis(6-(benzothien-2-yl)phenanthridinato)(4-methyl-4′-carboxypropyl-2,2′-bipyridine)iridium(III) ([Ir(btphen)$_2$]$_2$(bpy-COOH))[22] complexes,

[a]*Division of Nanobiomedicine, Suzhou Institute of Nano-Tech and Nano-Bionics, Chinese Academy of Sciences, 398 Ruoshui Road, Suzhou Industrial Park, Suzhou, Jiangsu 215123, P. R. China. E-mail: mzhou2007@sinano.ac.cn*
[b]*University of Chinese Academy of Sciences, 19A Yuquan Road, Beijing, 100049, P. R. China*
[c]*Institute of Chemistry, Chinese Academy of Sciences, 2 Zhongguancun North First Street, Beijing 100190, P. R. China*
[d]*SunaTech Inc., bioBAY, Suzhou Industrial Park, Suzhou, Jiangsu 215123, P. R. China*

†Electronic supplementary information (ESI) available: Ligand synthesis, absorption and emission of **IrMitoOlivine** and **IrMitoNIR** in PBS, and cell imaging of [Ir(bt)$_2$]$_2$(bpy-COOH) and [Ir(btphen)$_2$]$_2$(bpy-COOH). See DOI: 10.1039/c4dt00823e

‡Qingqing Zhang and Rui Cao contributed equally to this work.

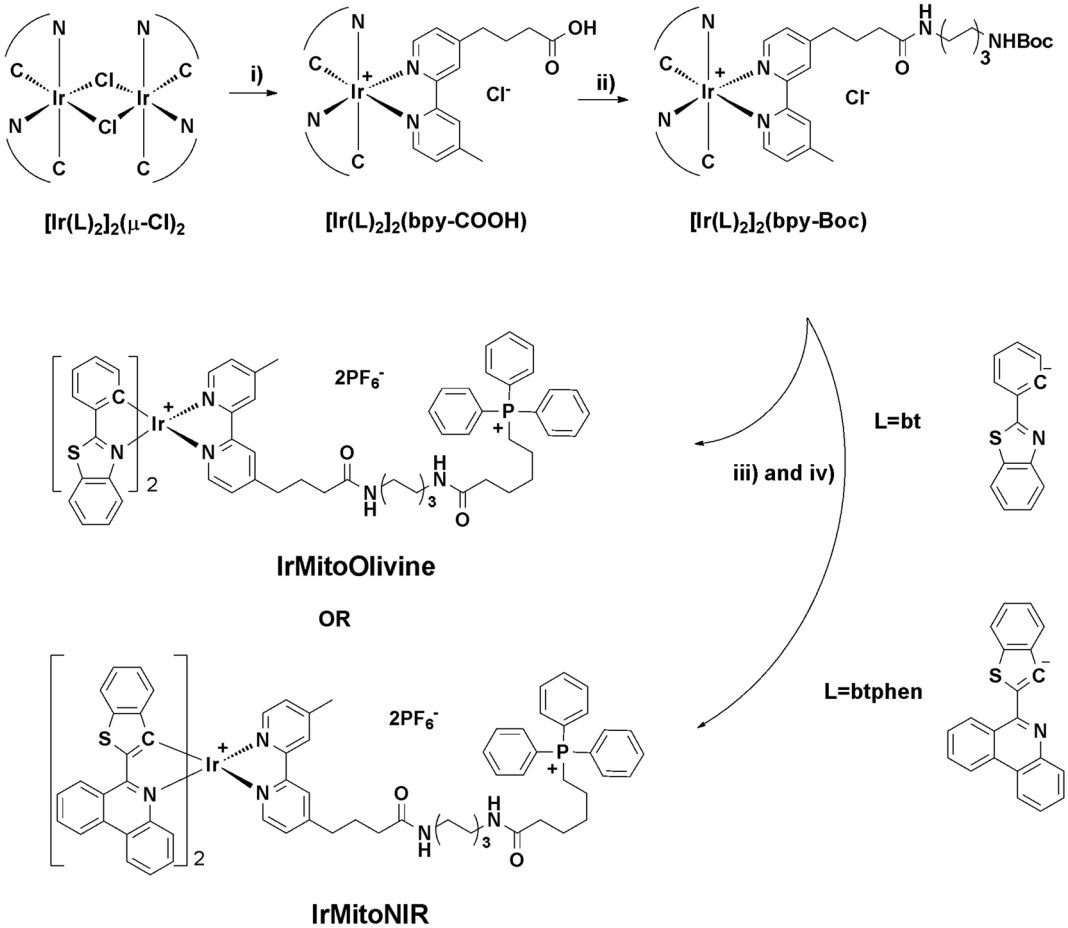

Scheme 1 Synthesis of **IrMitoOlivine** and **IrMitoNIR**. (i) MBBA, CH_2Cl_2–CH_3OH (50 vol%), 80 °C, 2–4 h; (ii) HDABoc; DCC–HOBt–DMF, r.t., 24 h; (iii) TFA–CH_2Cl_2 (20 vol%), r.t., 2 h; (iv) TPPC5H10COOH, DCC–HOBt–DMF, r.t., 24 h; NH_4PF_6.

were chosen as phosphorescent moieties, whose luminescence emission bands are distinct from those of commercially available MitoTracker® Red FM and Green FM, respectively. The two TPP functionalized probes, **IrMitoOlivine** and **IrMitoNIR**, were synthesized by conjugating carboxy terminals of the corresponding iridium(III) complex and TPP cation with the 1,6-hexamethylenediamine linker (Scheme 1), and characterized with high-resolution TOF-MS and $^1H/^{13}C$ NMR. Long linkage was employed to minimize the interplay of the phosphorescent emitter and the TPP cation.

Absorption and emission spectroscopy

The absorption and emission spectra of **IrMitoOlivine** and **IrMitoNIR** in CH_3CN are presented in Fig. 1, and the photophysical data are summarized in Table 1. As designed, **IrMitoOlivine** and **IrMitoNIR** exhibit yellowish green (λ_{em} 527, 563 nm) and NIR (λ_{em} 708 nm) phosphorescence with quantum yields Φ_{em} = 0.487 and 0.032 in N_2-saturated CH_3CN. Their ^{3}MLCT (metal-to-ligand charge transfer) absorption band lies in the range of 390–500 nm and 450–600 nm, respectively. In aqueous PBS buffer (Fig. S1†), the wavelengths of the absorption bands and emission peaks remained unchanged, but the quantum yields became smaller (0.039 and 0.013 for **IrMitoOlivine** and **IrMitoNIR**, respectively). In comparison with organic dyes, phosphorescent **IrMitoOlivine** and **IrMitoNIR** display complete separation of the emission

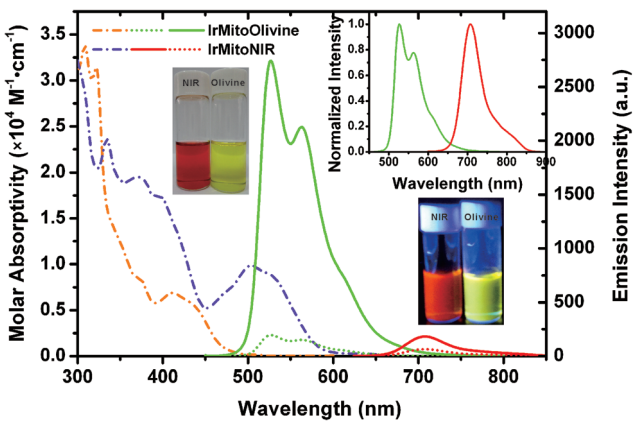

Fig. 1 Absorption (dash dot) and emission (solid: N_2-saturated; dot: air-saturated) spectra of **IrMitoOlivine** and **IrMitoNIR** in CH_3CN. The top right inset shows normalized emission spectra. Ex: **IrMitoOlivine**, 411 nm; **IrMitoNIR**, 504 nm. The photograph insets show the appearance of **IrMitoOlivine** and **IrMitoNIR** under natural (top left) and UV (bottom right) light, respectively.

Table 1 Photophysical data of **IrMitoOlivine** and **IrMitoNIR**

Compound	λ_{abs}/nm (ε/10^3 M^{-1} cm^{-1})		λ_{em}/nm	Φ_{em} [b]
IrMitoOlivine	CH_3CN[a]	309 (33.8), 322 (31.4), 381 (7.10, sh), 411 (6.88)	527, 563	0.487,[c] 0.035[d]
	PBS[e]	311 (32.3), 324 (29.7), 381 (7.86, sh), 414 (7.16)	526, 563	0.039
IrMitoNIR	CH_3CN[a]	334 (23.7), 370 (19.5), 394 (17.5, sh), 503 (5.83)	708	0.032,[c] 0.012[d]
	PBS[e]	336 (23.0), 373 (18.8), 396 (16.6, sh), 509 (9.02)	706	0.013

[a] Absorption and emission spectra were recorded in CH_3CN. [b] Quantum yields (Φ_{em}) were determined using $Ru(bpy)_3^{2+}$ (Φ_{em} = 0.062)[25] as the reference. [c] In N_2-saturated CH_3CN. [d] In air-saturated CH_3CN. [e] Absorption and emission spectra were recorded in DMSO–PBS (2 vol%).

bands from their ^{3}MLCT absorption regions, which brings an advantage in pairing the excitation light source and emission detection in a practical application. Though their emission intensities are sensitive to oxygen concentration (Φ_{em} 0.035 and 0.012 in air-saturated CH_3CN, respectively), phosphorescent IrMito dyes are still appropriate in most situations of biological research.

Lipophilicity and cytotoxicity

The lipophilicity (log D) of $[Ir(bt)_2]_2$(bpy-COOH), $[Ir(btphen)_2]_2$(bpy-COOH), **IrMitoOlivine** and **IrMitoNIR** was determined in the *n*-octanol–PBS (pH 7.4) system. The cytotoxicity of **IrMitoOlivine** and **IrMitoNIR** was evaluated using an MTT assay in HeLa cells. As expected, compared with $[Ir(bt)_2]_2$(bpy-COOH) and $[Ir(btphen)_2]_2$(bpy-COOH), which have a hydrophilic carboxy terminus, introduction of the lipophilic TPP cation increases the lipophilicity and thus the cytotoxicity of the delivered molecules.[9] **IrMitoOlivine** and **IrMitoNIR** showed relatively medium IC_{50} (**IrMitoOlivine** 38.7 ± 0.5 μM, **IrMitoNIR** 43.0 ± 0.3 μM) (Fig. 2 and Table 2). Therefore, we chose 20 μM of IrMito dyes in the following cell imaging.

Intracellular localization

To demonstrate **IrMitoOlivine** and **IrMitoNIR** specifically localizing in mitochondria, we performed co-localization imaging experiments using IrMito and MitoTracker® dyes to co-label HeLa cells. As given in Fig. 3, the observation showed confocal images of **IrMitoOlivine** (upper FITC channel) and **IrMitoNIR** (lower Cy5 channel) overlaid nearly completely with that of MitoTracker® Red FM (upper Cy5 channel) and Green FM (lower FITC channel), respectively, indicating both IrMito dyes targeted selectively mitochondria rather than other intracellular compartments or the cytoplasm. In comparison, $[Ir(bt)_2]_2$(bpy-COOH) and $[Ir(btphen)_2]_2$(bpy-COOH) (20 μM, 5% DMSO) were used to stain the HeLa cells through a similar procedure for 2 h (Fig. S2†). The result revealed that, without the TPP moiety, $[Ir(bt)_2]_2$(bpy-COOH) and $[Ir(btphen)_2]_2$(bpy-COOH) were still able to permeate into the cell but were well-distributed in the cytoplasm, even though more concentrated around the nucleus and little distributed in the nucleus.

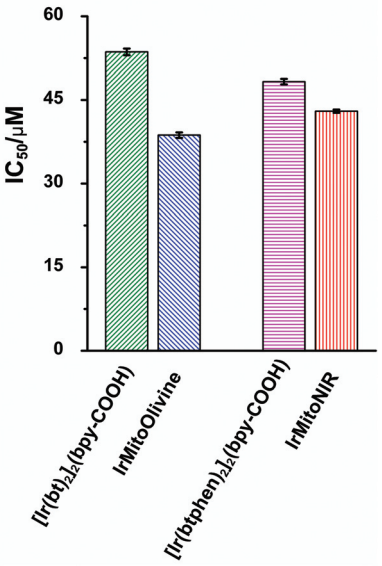

Fig. 2 Cytotoxicity (IC_{50}) of **IrMitoOlivine** and **IrMitoNIR** in HeLa cells.

Table 2 Cytotoxicity and lipophilicity of **IrMitoOlivine** and **IrMitoNIR**

Compound	IC_{50}/μM	Log D[a]
$[Ir(bt)_2]_2$(bpy-COOH)	53.6 ± 0.6	1.03 ± 0.03
IrMitoOlivine	38.7 ± 0.5	1.38 ± 0.05
$[Ir(btphen)_2]_2$(bpy-COOH)	48.3 ± 0.5	1.27 ± 0.05
IrMitoNIR	43.0 ± 0.3	1.52 ± 0.04

[a] Log D = log[C_o'/(C_o − C_o')], where C_o and C_o' are the molar concentrations of the analyte in the *n*-octanol phase (saturated with PBS) before and after partition.

Anti-photobleaching

The photostability of **IrMitoOlivine** and **IrMitoNIR** compared with organic dyes under continuous laser irradiation was determined using time-lapse imaging of IrMito and MitoTracker® co-stained HeLa cells. Time-lapse imaging proceeded for 100 s with 20 s intervals. As shown in Fig. 4, the phosphorescence intensity of IrMito dyes (Fig. 4c, FITC, and 4d, Cy5 channels) remained almost constant (see IrMitoOlivine.avi and IrMitoNIR.avi in ESI†), while the fluorescence of MitoTracker® decreased significantly (MitoTrackerRed.avi and MitoTrackerGreen.avi in ESI†), especially for MitoTracker® Red FM. For the quantitative analysis, the photobleaching factor was defined as follows:

$$\text{Photobleaching factor} = \frac{I_t - I_{B,t}}{I_0 - I_{B,0}}$$

I_t, $I_{B,t}$, I_0, $I_{B,0}$ are fluorescence intensities at the time t and the time of starting the measurements, respectively; the

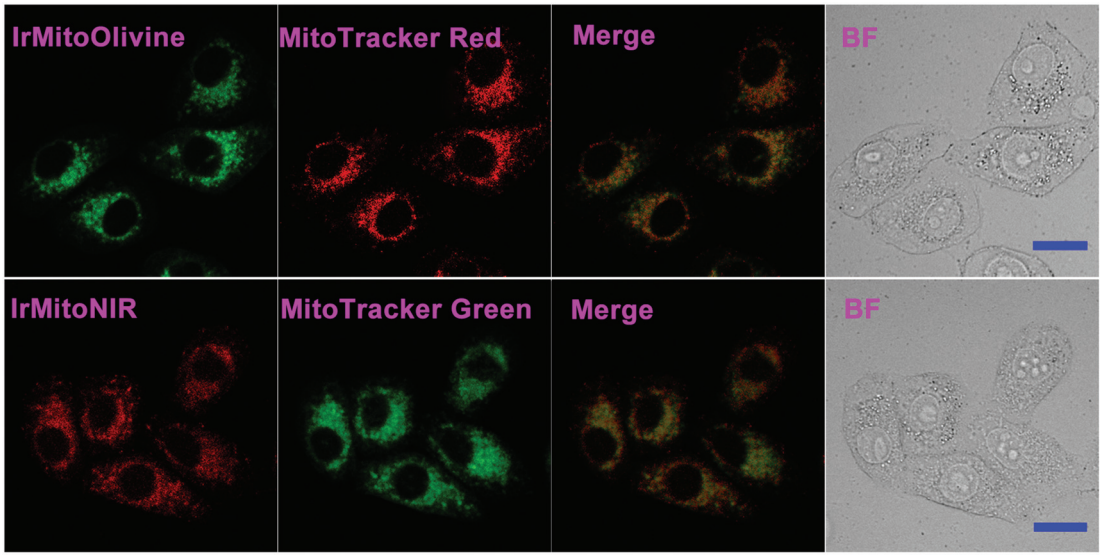

Fig. 3 Cell imaging of **IrMitoOlivine** and **IrMitoNIR** showing co-localization of MitoTracker® and IrMito dyes in HeLa cells. Channel: FITC, Ex 488 nm, Em 500–530 nm; Cy5, Ex 561 nm, Em 662–737 nm. Scale bar: 20 mm.

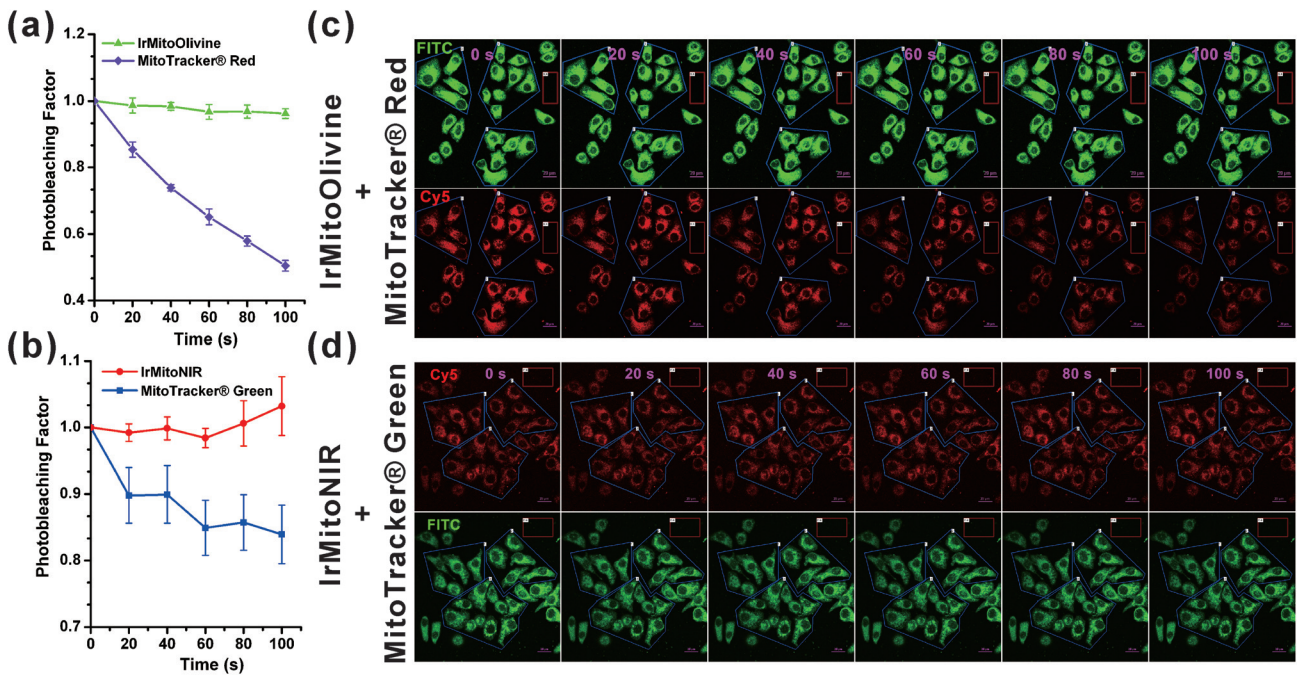

Fig. 4 Anti-photobleaching observation of **IrMitoOlivine** and **IrMitoNIR** in HeLa cells. (a, b) Quantitative photobleaching results showed that **IrMitoOlivine** and **IrMitoNIR** possessed robust emission intensity under continuous light irradiation. The data were presented as mean ± standard deviation. (c, d) Time-lapse confocal imaging of **IrMitoOlivine**/MitoTracker® Red FM or **IrMitoNIR**/MitoTracker® Green FM co-stained HeLa cells. Blue and red ROIs represent three stochastically chosen cell-inclusive regions and the background region, respectively. Time interval: 20 s. Scale bar: 20 mm.

subscript B denotes background fluorescence intensity. Three cell-inclusive and one background regions were randomly chosen to quantify their fluorescence intensity with the Nikon NIS-Elements AR software. Quantitative anti-photobleaching analysis indicated that the statistical emission intensity of **IrMitoOlivine** and **IrMitoNIR** retained a high stability with a small fluctuation of less than 5%; however, the fluorescence intensities of the commercial MitoTracker® Red FM and Green FM diminished obviously, up to 50% and 16%, respectively, at the end of the measurements. The result showed that mitochondria-targetable phosphorescent dyes are potentially promising in long-time quantitative imaging in living cells owing to their excellent anti-photobleaching capability even under continuous exposure to laser.

Experimental section

General information

1,6-Hexylenediamine, 6-bromocaproic acid and di-*tert*-butyl dicarbonate (Boc_2O) were purchased from Aladdin, triphenylphosphine and *n*-octanol from Sinopharm, DCC and MTT from Sigma-Aldrich, and HOBt from GL Biochem. MitoTracker® Red FM and MitoTracker® Green FM were received from Life Technologies. 4-(4′-Methyl-2,2′-bipyridin-4-yl)butyric acid (MBBA), $[Ir(bt)_2]_2(\mu\text{-}Cl)_2$ and $[Ir(btphen)_2]_2(\mu\text{-}Cl)_2$ were synthesized with the method described in the literature (ESI†). Other chemicals and solvents were commercially available in analytical grade and were used directly unless otherwise specified.

Human cervical carcinoma HeLa cells were received from the Institute of Biochemistry and Cell Biology, SIBS, CAS. DMEM (Dulbecco's modified Eagle medium), FBS (fetal bovine serum) and penicillin/streptomycin were purchased from Sigma-Aldrich.

GC-MS spectra were determined on an Agilent 7890A GC system equipped with a 5975C inert triple-axel MS detector. ESI-TOF-MS spectra were measured on an Agilent 1200/6200 TOF-MS system. ^1H and ^{13}C NMR spectra were acquired from a Varian 400 MHz NMR spectrometer. Elemental analysis (C, N, H) was performed on a Vario EL III Element Analyzer (Elementar). UV-Visible absorption and emission spectra were measured on a Lambda 25 UV/Vis spectrometer (PerkinElmer) and an F4600 fluorescence spectrophotometer (Hitachi), respectively.

6-Carboxypentamethylenetriphenylphosphonium bromide (TPPC5H10COOH). TPPC5H10COOH was synthesized as described by Manning *et al.*[23] A mixture of triphenylphosphine (7.42 g, 28.3 mmol) and 6-bromocaproic acid (5.01 g, 25.7 mmol) in xylene (35 ml) was placed in a 100 ml round-bottomed flask equipped with a water-cooled condenser. The solution was heated to reflux for 4 hours with vigorous stirring until the solution turned turbid and separated into two phases. When the temperature of the solution was down to 40–50 °C, diethyl ether (30 ml) was added slowly with vigorous stirring to give off-white microcrystals, which were collected by vacuum filtration. The product was washed with diethyl ether twice and then dried *in vacuo* to afford a white solid (6.28 g, yield 50.5%). ESI-TOF-MS: *m*/*z* ($[M - Br]^+$) calcd 377.1670, found 377.1654. ^1H NMR (400 MHz, $CDCl_3$) δ 7.88–7.62 (m, 15H), 3.56 (s, 2H), 2.45–2.27 (m, 2H), 1.64 (s, 6H). ^{13}C NMR (101 MHz, $CDCl_3$) δ 176.0, 135.1, 132.0 (dd, J = 297.3, 11.2 Hz), 117.9 (d, J = 86.0 Hz), 34.0, 29.4 (d, J = 16.1 Hz), 23.9, 22.3 (d, J = 51.1 Hz), 21.9; ^{31}P NMR (162 MHz, $CDCl_3$) δ 23.9.

***tert*-Butyl 6-aminohexylcarbamate (HDABoc).** HDABoc was synthesized according to Dardonville *et al.*[24] To a CH_2Cl_2 solution of 1,6-hexylenediamine (20.06 g, 172.6 mmol) was added dropwise di-*tert*-butyl dicarbonate (7.6 g, 34.8 mmol) dissolved in CH_2Cl_2. After 20 h of stirring at room temperature, the mixture was filtered. The filtrate was concentrated and re-dissolved in ethyl acetate, and washed with water. Removal of the solvent gave a milky liquid (5.36 g, yield 71.2%). GC-MS: *m*/*z* ($[M - Bu^t]^+$) calcd 159.11, found 159.1. ^1H NMR (400 MHz, $CDCl_3$): δ 4.66 (s, 1H), 3.10 (d, J = 6.3 Hz, 2H), 2.68 (t, J = 6.9 Hz, 2H), 1.44 (s, 9H), 1.52–1.22 (m, 10H).

$[Ir(bt)_2]_2$(bpy-COOH) and $[Ir(btphen)_2]_2$(bpy-COOH). $[Ir(bt)_2]_2$(bpy-COOH) and $[Ir(btphen)_2]_2$(bpy-COOH) were synthesized in a similar manner. $[Ir(bt)_2]_2$(bpy-COOH): a mixture of $[Ir(bt)_2]_2(\mu\text{-}Cl)_2$ (950 mg, 0.77 mmol) and MBBA (421 mg, 1.64 mmol) was refluxed at 80 °C in CH_2Cl_2–CH_3OH mixed solvent until the solution turned transparent (*ca.* 2 h). After evaporating of solvents, the product was separated by silica gel column chromatography (gradient elution with CH_2Cl_2–CH_3OH) to afford orange crystals (1.23 g, yield 89.2%). ESI-TOF-MS: *m*/*z* ($[M - Cl]^+$) calcd 869.1596, found 869.1595. ^1H NMR (400 MHz, $CDCl_3$) δ 9.32 (s, 1H), 9.01 (s, 1H), 7.90–7.75 (m, 5H), 7.40–7.31 (m, 3H), 7.27 (d, J = 7.4 Hz, 2H), 7.21 (d, J = 5.7 Hz, 1H), 7.14–7.02 (m, 3H), 6.89–6.81 (m, 2H), 6.38 (dd, J = 7.6, 3.1 Hz, 2H), 6.32–6.27 (m, 1H), 6.25 (d, J = 8.4 Hz, 1H), 2.97 (dt, J = 21.7, 6.9 Hz, 2H), 2.75–2.59 (m, 5H), 2.22 (dd, J = 13.0, 6.6 Hz, 2H); ^{13}C NMR (101 MHz, $CDCl_3$) δ 181.0, 180.8, 175.0, 156.6, 156.4, 155.9, 152.8, 150.7, 149.9, 149.4, 149.2, 149.1, 140.2, 140.1, 133.4, 133.3, 132.1, 132.0, 131.3, 131.0, 128.8, 128.7, 128.3, 128.2, 126.7, 126.6, 126.5, 126.1, 125.9, 125.8, 123.5, 123.3, 123.1, 123.0, 117.9, 117.7, 34.6, 34.3, 25.5, 21.4. Elemental analysis ($C_{41}H_{32}N_4O_2S_2ClIr$, %): calcd C 54.44, H 3.57, N 6.09; found C 54.20, H 3.65, N 6.07. $[Ir(btphen)_2]_2$(bpy-COOH): $[Ir(btphen)_2]_2(\mu\text{-}Cl)_2$ (867 mg, 0.51 mmol) and MBBA (264 mg, 1.03 mmol) were dissolved in CH_2Cl_2–CH_3OH solution, and refluxed to turn transparent. After filtration and removal of solvents, the residue was separated similarly to $[Ir(bt)_2]_2$(bpy-COOH) to afford dark red crystals (925 mg, yield 82.1%). ESI-TOF-MS: *m*/*z* ($[M - Cl]^+$) calcd 1069.2222, found 1069.2227. ^1H NMR (400 MHz, $CDCl_3$) δ 9.39 (s, 2H), 8.61 (s, 2H), 8.46 (s, 1H), 8.28 (s, 5H), 8.03–7.81 (m, 6H), 7.18 (dt, J = 44.0, 12.8 Hz, 10H), 6.71 (dd, J = 23.8, 14.8 Hz, 6H), 2.65 (s, 2H), 2.39 (s, 5H), 1.87 (s, 2H); ^{13}C NMR (101 MHz, $CDCl_3$) δ 175.2, 167.9, 167.8, 159.5, 159.2, 156.3, 155.1, 155.0, 152.8, 145.6, 145.5, 143.7, 143.6, 143.5, 138.6, 138.4, 133.7, 133.6, 133.3, 128.9, 128.7, 128.4, 128.1, 127.9, 127.8, 127.7, 127.3, 127.0, 126.9, 126.7, 125.6, 125.4, 124.8, 124.7, 124.1, 124.0, 122.9, 122.8, 122.8, 122.7, 122.7, 122.6, 122.1, 122.0, 34.1, 34.0, 25.5, 21.1. Elemental analysis ($C_{57}H_{40}N_4O_2S_2ClIr$, %): calcd C 61.97, H 3.65, N 5.07; found C 61.76, H 3.70, N 5.05.

$[Ir(bt)_2]_2$(bpy-Boc) and $[Ir(btphen)_2]_2$(bpy-Boc). $[Ir(bt)_2]_2$(bpy-Boc) and $[Ir(btphen)_2]_2$(bpy-Boc) were synthesized similarly. $[Ir(bt)_2]_2$(bpy-Boc): a mixture of $[Ir(bt)_2]_2$(bpy-COOH) (361 mg, 0.40 mmol), HDABoc (130 mg, 0.60 mmol), DCC (203 mg, 0.98 mmol) and HOBt (65 mg, 0.48 mmol) was stirred in 10 ml of anhydrous DMF at room temperature under N_2 protection overnight. After freezing, filtration and removal of the solvent, the residual solid was separated prudently by silica gel column chromatography (CH_2Cl_2–C_2H_5OH = 20 : 1) to afford a yellow powder (382 mg, yield 86.6%). ESI-TOF-MS: *m*/*z* ($[M - Cl]^+$) calcd 1067.3328, found 1067.3298. ^1H NMR (400 MHz, $CDCl_3$) δ 8.52 (d, J = 7.2 Hz, 2H), 7.87 (ddd, J = 10.1, 9.6, 5.6 Hz, 4H), 7.79 (ddd, J = 7.7, 4.4, 0.8 Hz, 2H), 7.39–7.30 (m, 3H), 7.28–7.23 (m, 1H), 7.14 (td, J = 8.4, 1.0 Hz, 2H), 7.09–7.03 (m, 2H), 6.85 (dd, J = 10.8, 4.2 Hz, 2H), 6.37 (d, J = 7.7 Hz, 2H), 6.20 (d, J = 8.4 Hz, 1H), 6.13 (d, J = 8.4 Hz, 1H), 3.11 (dd, J = 12.7, 6.7 Hz, 2H), 3.04 (t, J = 6.8 Hz, 2H), 2.89 (t,

J = 7.7 Hz, 2H), 2.62 (s, 3H), 2.38 (t, J = 7.5 Hz, 2H), 2.12–2.01 (m, 2H), 1.43 (s, 13H), 1.23 (s, 4H). $[Ir(btphen)_2]_2$(bpy-Boc): the mixture of $[Ir(btphen)_2]_2$(bpy-COOH) (113 mg, 0.102 mmol), HDABoc (49.8 mg, 0.230 mmol), DCC (71.4 mg, 0.346 mmol) and HOBt (15.4 mg, 0.116 mmol) was dissolved in super-dry DMF (5 ml) and reacted at 0 °C for 24 h. The purification procedure used was similar to that for $[Ir(bt)_2]_2$(bpy-Boc). Dark red powder (112 mg, yield 84.3%). ESI-TOF-MS: m/z ($[M - Cl]^+$) calcd 1267.3954, found 1267.3967. ^{1}H NMR (400 MHz, $CDCl_3$) δ 9.44–9.35 (m, 2H), 8.78 (s, 1H), 8.64–8.56 (m, 2H), 8.27 (dd, J = 11.6, 5.7 Hz, 4H), 8.04–7.91 (m, 5H), 7.87 (d, J = 7.7 Hz, 2H), 7.71 (dd, J = 24.8, 8.4 Hz, 1H), 7.35–7.12 (m, 5H), 7.07 (dd, J = 22.3, 5.7 Hz, 2H), 6.81–6.60 (m, 6H), 3.00 (d, J = 6.2 Hz, 2H), 2.64 (s, 2H), 2.39 (d, J = 4.3 Hz, 3H), 2.23 (d, J = 7.1 Hz, 2H), 1.89 (s, 2H), 1.55–1.06 (m, 19H).

IrMitoOlivine and IrMitoNIR. **IrMitoOlivine** and **IrMitoNIR** were synthesized with a similar method. **IrMitoOlivine**: after de-protection of $[Ir(bt)_2]_2$(bpy-Boc) (253 mg, 0.229 mmol), the residue was stirred with TPPC5H10COOH (158 mg, 0.346 mmol), DCC (119 mg, 0.577 mmol) and HOBt (38.2 mg, 0.282 mmol) in anhydrous DMF (7.5 ml) at room temperature for 24 h. Then 30 ml of saturated NH_4PF_6 aqueous solution was added to precipitate the product. The filtrate was then separated by silica gel column chromatography (gradient elution with CH_2Cl_2–CH_3OH). Yellow crystals, 268 mg, yield 72.4%. ESI-TOF-MS: m/z ($[M - 2PF_6]^{2+}$) calcd 663.2185, found 663.2157. ^{1}H NMR (400 MHz, $CDCl_3$) δ 8.47 (d, J = 3.9 Hz, 1H), 8.42 (d, J = 2.0 Hz, 1H), 7.91 (dt, J = 14.1, 7.5 Hz, 4H), 7.83–7.73 (m, 5H), 7.73–7.61 (m, 15H), 7.57–7.52 (m, 1H), 7.50–7.43 (m, 1H), 7.38–7.28 (m, 4H), 7.18–7.09 (m, 2H), 7.08–6.99 (m, 2H), 6.87–6.78 (m, 2H), 6.38 (dd, J = 9.8, 2.3 Hz, 2H), 6.26–6.18 (m, 1H), 6.12 (dd, J = 15.0, 8.4 Hz, 1H), 3.29 (dd, J = 14.0, 7.1 Hz, 2H), 3.08 (ddd, J = 22.8, 19.7, 9.9 Hz, 6H), 2.91 (d, J = 34.4 Hz, 2H), 2.58 (d, J = 3.1 Hz, 3H), 2.39 (t, J = 7.4 Hz, 1H), 2.28 (t, J = 7.2 Hz, 3H), 2.13 (dd, J = 14.3, 7.3 Hz, 2H), 2.01 (dd, J = 13.8, 6.7 Hz, 2H), 1.64 (s, 10H); ^{13}C NMR (101 MHz, $CDCl_3$) δ 181.1, 177.3, 174.6, 173.9, 173.6, 173.2, 156.6, 156.4, 156.2, 156.1, 156.0, 155.9, 152.7, 150.4, 150.2, 149.8, 149.1, 149.0, 140.1, 139.0, 135.2, 133.3, 133.2, 132.0, 131.9, 131.8, 131.3, 130.6, 130.5, 128.8, 128.7, 128.5, 128.2, 127.4, 126.7, 126.6, 126.0, 123.6, 123.1, 118.2, 117.3, 116.2, 111.6, 77.6, 77.5, 77.3, 77.0, 53.7, 42.5, 40.6, 39.5, 38.6, 35.7, 33.4, 33.0, 32.3, 29.5, 29.3, 28.6, 26.6, 26.0, 25.2, 24.7, 24.5, 23.8, 22.1, 22.0, 21.6, 21.2, 14.1, 12.8; ^{31}P NMR (162 MHz, $CDCl_3$) δ 23.2. Elemental analysis ($C_{71}H_{70}F_{12}N_6O_2P_3S_2Ir$, %): calcd C 52.75, H 4.36, N 5.20; found C 52.63, H 4.42, N 5.08. **IrMitoNIR**: a mixture of de-protected $[Ir(btphen)_2]_2$(bpy-Boc) (65.2 mg, 54.2 μmol), TPPC5H10COOH (37.8 mg, 82.9 μmol), DCC (25 mg, 121 μmol) and HOBt (9.25 mg, 68.5 μmol) was stirred in super-dry DMF (3 ml) under inert gas protection at 0 °C for 24 h. After precipitation in saturated NH_4PF_6 solution (30 ml), the solid was then separated by silica gel column chromatography (gradient elution with CH_2Cl_2–CH_3OH) to afford red crystals (61.2 mg, yield 62.1%). ESI-TOF-MS: m/z ($[M - 2PF_6]^{2+}$) calcd 763.2498, found 763.2516. ^{1}H NMR (400 MHz, $CDCl_3$) δ 9.43–9.36 (m, 2H), 8.66–8.56 (m, 2H), 8.41–8.26 (m, 4H), 8.03–7.94 (m, 4H), 7.92 (s, 1H), 7.89–7.83 (m, 3H), 7.78 (dd, J = 10.2, 4.5 Hz, 3H), 7.73–7.59 (m, 13H), 7.32–7.27 (m, 2H), 7.15 (dddd, J = 14.5, 11.2, 9.5, 4.1 Hz, 5H), 6.72 (dd, J = 13.6, 7.8 Hz, 4H), 6.65 (dd, J = 11.3, 4.0 Hz, 2H), 3.31–2.99 (m, 8H), 2.66–2.54 (m, 2H), 2.33 (s, 5H), 2.23 (s, 4H), 1.76 (d, J = 27.9 Hz, 2H), 1.72–1.53 (m, 10H); ^{13}C NMR (101 MHz, $CDCl_3$) δ 177.7, 176.9, 173.7, 173.0, 172.1, 167.9, 165.8, 163.1, 159.2, 159.1, 154.9, 154.8, 152.7, 146.3, 145.6, 143.6, 139.5, 138.6, 138.5, 135.2, 133.3, 133.2, 131.9, 131.8, 130.6, 130.5, 128.8, 128.6, 128.4, 127.9, 127.0, 126.7, 125.4, 124.9, 124.7, 124.0, 122.8, 122.6, 122.1, 118.2, 117.3, 116.6, 111.4, 53.6, 42.5, 40.6, 38.6, 34.9, 33.5, 32.3, 29.7, 29.6, 29.5, 29.4, 29.3, 26.0, 24.5, 24.3, 23.8, 22.2, 22.1, 22.0, 21.8, 21.7, 21.6, 14.1, 12.9, 53.6, 42.5, 40.6, 38.6, 34.9, 33.5, 32.3, 29.7, 29.6, 29.5, 29.4, 29.3, 26.0, 24.5, 24.3, 23.8, 22.2, 22.1, 22.0, 21.8, 21.7, 21.6, 14.1, 12.9; ^{31}P NMR (162 MHz, $CDCl_3$) δ 23.3. Elemental analysis ($C_{87}H_{78}F_{12}N_6O_2P_3S_2Ir$, %): calcd C 57.51, H 4.33, N 4.63; found C 57.34, H 4.18, N 4.58.

Absorption and emission spectroscopy

The absorption and emission spectra were recorded in CH_3CN (UPLC grade, Acros) and DMSO–PBS (2 vol%) at room temperature. Quantum yields of **IrMitoOlivine** and **IrMitoNIR** were determined in N_2- and air-saturated CH_3CN and DMSO–PBS (2 vol%) with $Ru(bpy)_3^{2+}$ in aerated CH_3CN as a reference (Φ = 0.062),[25] and calculated with the following equation:

$$\Phi_{sam} = \Phi_{ref} \times \frac{I_{sam}}{I_{ref}} \times \frac{A_{ref}}{A_{sam}} \times \frac{{n_{sam}}^2}{{n_{ref}}^2}$$

where Φ, I, A, and n are the quantum yield, integral emission intensity, absorbance and refractive index of the solvents in which the sample or reference dissolved, respectively.

Lipophilicity

The lipophilicity of **IrMitoOlivine** and **IrMitoNIR** was determined in the n-octanol–PBS (pH 7.4) system using the conventional flask-shaking method, which was expressed as $\log D$ for ionized compounds. PBS and n-octanol were mixed vigorously for 24 h and then the mixture stood still for another 24 h to saturate each other. The excessive analyte was dissolved in the n-octanol (saturated with PBS) phase for 24 h to obtain a saturated solution, whose concentration was denoted C_o. The saturated n-octanol solution was then mixed with an equal volume of PBS (saturated with n-octanol) and shaken in an oscillator for 24 h. After partition, the concentration in the n-octanol phase was denoted C'_o. The lipophilicity $\log D$ was calculated with the following equation: $\log D = \log[C'_o/(C_o - C'_o)]$. The concentration was measured with fluorescence spectrophotometry (**ItMitoOlivine**: Ex 411 nm, Em 526; **IrMitoNIR**: Ex 504 nm, Em 708 nm). The data were determined in triplicate and expressed as mean ± standard deviation.

MTT assay

An MTT assay of **IrMitoOlivine** and **IrMitoNIR** in HeLa cells was carried out to detect their cytotoxicity. HeLa cells (*ca.* 1×10^4 cells per well) in the exponential phase were seeded

into a 96-well plate (Corning) and incubated in DMEM supplemented with 10% FBS containing 1% penicillin/streptomycin for 24 h before treatment. **IrMitoOlivine** or **IrMitoNIR** in DMSO (100–3.13 μM) were mixed into 1 mL fresh DMEM–FBS and added to each well and incubated for another 24 h at 37 °C under a 5% CO_2 environment. Furthermore, MTT (3-(4,5-dimethylthiazol-2-yl)-2,5-diphenyltetrazolium bromide) in PBS buffer (5 mg ml^{-1}) was added and the cells were grown for a further 4 h. After removal of the MTT solution, 150 μl of DMSO was added to each well and incubated at 37 °C for 15 min. The OD_{490} value of each sample was measured with a Victor X4 microplate reader (Perkin-Elmer). The assay was performed three times independently and in triplicate each time. IC_{50} values were calculated in SPSS 18 and presented as mean ± standard deviation.

Cell staining

HeLa cells were plated on a 35 mm cell culture dish (Corning) at a density of 1–2 × 10^4 cells per dish. After incubation for 24 h at 37 °C under 5% CO_2, cells were co-stained with **IrMitoOlivine** (20 μM)/MitoTracker® Red FM (200 nM) or **IrMitoNIR** (20 μM)/MitoTracker® Green RM (100 nM) in 1 ml DMEM–FBS medium for 30 min, respectively. After replacement with fresh medium, the cells were imaged with a Nikon A1R confocal laser scanning microscope for intracellular localization of IrMito dyes. Moreover, for the *in vivo* anti-photobleaching assay of IrMito dyes, time-lapse cell images were collected continuously with 20 s intervals for 100 s. Fluorescence intensities of three stochastically chosen cell-inclusive regions were acquired with the NIS-Elements AR software (Nikon), and their photobleaching factors were calculated. The data were presented as mean ± standard deviation.

Conclusion

In conclusion, two phosphorescent iridium(III) complexes conjugated with a lipophilic triphenylphosphonium cation, **IrMitoOlivine** and **IrMitoNIR**, were rationally designed and synthesized. Both complexes demonstrated specificity to mitochondria. Quantitative photobleaching analysis revealed their excellent anti-photobleaching capability in continuous living cell imaging. In particular, we demonstrated a facile method of combining intracellular compartment specificity with the chemically stable phosphorescent iridium(III) complexes, making such phosphorescent metal complexes promising for building up more organelle-targeting probes.

Acknowledgements

This work was financially supported by the Natural Science Foundation of China (grant no. 21005084 and 21072218). We thank Wanfei Li for his suggestive directions in the synthesis of ligands.

Notes and references

1 (*a*) G. C. Kujoth, A. Hiona, T. D. Pugh, S. Someya, K. Panzer, S. E. Wohlgemuth, T. Hofer, A. Y. Seo, R. Sullivan, W. A. Jobling, J. D. Morrow, H. Van Remmen, J. M. Sedivy, T. Yamasoba, M. Tanokura, R. Weindruch, C. Leeuwenburgh and T. A. Prolla, *Science*, 2005, **309**, 481–484; (*b*) M. T. Lin and M. F. Beal, *Nature*, 2006, **443**, 787–795; (*c*) E. Cadenas and K. J. A. Davies, *Free Radicals Biol. Med.*, 2000, **29**, 222–230.

2 (*a*) D. R. Green and J. C. Reed, *Science*, 1998, **281**, 1309–1312; (*b*) G. Kroemer, B. Dallaporta and M. Resche-Rigon, *Annu. Rev. Physiol.*, 1998, **60**, 619–642; (*c*) X. Wang, *Genes Dev.*, 2001, **15**, 2922–2933.

3 (*a*) L. B. Chen, *Annu. Rev. Cell Biol.*, 1988, **4**, 155–181; (*b*) M. P. Murphy, *Trends Biotechnol.*, 1997, **15**, 326–330.

4 S. Davis, M. J. Weiss, J. R. Wong, T. J. Lampidis and L. B. Chen, *J. Biol. Chem.*, 1985, **260**, 13844–13850.

5 For example, Rhodamine 123; L. V. Johnson, M. L. Walsh and L. B. Chen, *Proc. Natl. Acad. Sci. U. S. A.*, 1980, **77**, 990–994. MitoTracker® Orange CMTMRos and Red CMXRos available from Life Technologies also belong to this class.

6 For example, JC-1; M. Reers, T. W. Smith and L. B. Chen, *Biochemistry*, 1991, **30**, 4480–4486. MitoTracker® Green FM, Red FM and Deep Red FM, available from Life Technologies, also belong to this class.

7 R. A. J. Smith, C. M. Porteous, A. M. Gane and M. P. Murphy, *Proc. Natl. Acad. Sci. U. S. A.*, 2003, **100**, 5407–5412.

8 M. P. Murphy and R. A. J. Smith, *Annu. Rev. Pharmacol. Toxicol.*, 2007, **47**, 629–656.

9 M. P. Murphy and R. A. J. Smith, *Adv. Drug Delivery Rev.*, 2000, **41**, 235–250.

10 A. Muratovska, R. N. Lightowlers, R. W. Taylor, J. A. Wilce and M. P. Murphy, *Adv. Drug Delivery Rev.*, 2001, **49**, 189–198.

11 (*a*) D.-Y. Kim, H.-J. Kim, K.-H. Yu and J.-J. Min, *Bioconjugate Chem.*, 2012, **23**, 431–437; (*b*) Y. Zhou and S. Liu, *Bioconjugate Chem.*, 2011, **22**, 1459–1472.

12 (*a*) K. Sreenath, J. R. Allen, M. W. Davidson and L. Zhu, *Chem. Commun.*, 2011, **47**, 11730–11732; (*b*) G. Masanta, C. S. Lim, H. J. Kim, J. H. Han, H. M. Kim and B. R. Cho, *J. Am. Chem. Soc.*, 2011, **133**, 5698–5700; (*c*) N. Y. Baek, C. H. Heo, C. S. Lim, G. Masanta, B. R. Cho and H. M. Kim, *Chem. Commun.*, 2012, **48**, 4546–4548.

13 (*a*) B. C. Dickinson and C. J. Chang, *J. Am. Chem. Soc.*, 2008, **130**, 9638–9639; (*b*) B. C. Dickinson, D. Srikun and C. J. Chang, *Curr. Opin. Chem. Biol.*, 2010, **14**, 50–56; (*c*) G. Masanta, C. H. Heo, C. S. Lim, S. K. Bae, B. R. Cho and H. M. Kim, *Chem. Commun.*, 2012, **48**, 3518–3520.

14 (*a*) C. Adachi, M. A. Baldo, M. E. Thompson and S. R. Forrest, *J. Appl. Phys.*, 2001, **90**, 5048–5051; (*b*) M. Yu, Q. Zhao, L. Shi, F. Li, Z. Zhou, H. Yang, T. Yi and C. Huang, *Chem. Commun.*, 2008, 2115–2117; (*c*) Y. Chen, L. Qiao, B. Yu, G. Li, C. Liu, L. Ji and H. Chao, *Chem. Commun.*, 2013, **49**, 11095–11097.

15 (*a*) H. Chen, Q. Zhao, Y. Wu, F. Li, H. Yang, T. Yi and C. Huang, *Inorg. Chem.*, 2007, **46**, 11075–11081; (*b*) D.-L. Ma, W.-L. Wong, W.-H. Chung, F.-Y. Chan, P.-K. So, T.-S. Lai, Z.-Y. Zhou, Y.-C. Leung and K.-Y. Wong, *Angew. Chem., Int. Ed.*, 2008, **47**, 3735–3739; (*c*) Q. Zhao, F. Li and C. Huang, *Chem. Soc. Rev.*, 2010, **39**, 3007–3030; (*d*) Y. You, S. Cho and W. Nam, *Inorg. Chem.*, 2014, **53**, 1804–1815; (*e*) M. Marín-Suárez, B. F. E. Curchod, I. Tavernelli, U. Rothlisberger, R. Scopelliti, I. Jung, D. Di Censo, M. Grätzel, J. F. Fernández-Sánchez, A. Fernández-Gutiérrez, M. K. Nazeeruddin and E. Baranoff, *Chem. Mater.*, 2012, **24**, 2330–2338; (*f*) Y. You, Y. Han, Y.-M. Lee, S. Y. Park, W. Nam and S. J. Lippard, *J. Am. Chem. Soc.*, 2011, **133**, 11488–11491.

16 (*a*) Q. Zhao, M. Yu, L. Shi, S. Liu, C. Li, M. Shi, Z. Zhou, C. Huang and F. Li, *Organometallics*, 2010, **29**, 1085–1091; (*b*) X. Wang, J. Jia, Z. Huang, M. Zhou and H. Fei, *Chem. – Eur. J.*, 2011, **17**, 8028–8032; (*c*) Q. Zhao, C. Huang and F. Li, *Chem. Soc. Rev.*, 2011, **40**, 2508–2524.

17 S. P.-Y. Li, C. T.-S. Lau, M.-W. Louie, Y.-W. Lam, S. H. Cheng and K. K.-W. Lo, *Biomaterials*, 2013, **34**, 7519–7532.

18 (*a*) T. Murase, T. Yoshihara and S. Tobita, *Chem. Lett.*, 2012, **41**, 262–263; (*b*) T. Yoshihara, A. Kobayashi, S. Oda, M. Hosaka, T. Takeuchi and S. Tobita, in *Proc. SPIE 8233, Reporters, Markers, Dyes, Nanoparticles, and Molecular Probes for Biomedical Applications IV*, San Francisco, CA, USA, 2012, pp. 82330A–882338.

19 (*a*) Y. Li, Y. Liu and M. Zhou, *Dalton Trans.*, 2012, **41**, 3807–3816; (*b*) E. Baranoff, B. F. E. Curchod, J. Frey, R. Scopelliti, F. Kessler, I. Tavernelli, U. Rothlisberger, M. Grätzel and M. K. Nazeeruddin, *Inorg. Chem.*, 2011, **51**, 215–224; (*c*) Y. Zhou, W. Li, Y. Liu and M. Zhou, *ChemPlusChem*, 2013, **78**, 413–418.

20 (*a*) L. Xiong, Q. Zhao, H. Chen, Y. Wu, Z. Dong, Z. Zhou and F. Li, *Inorg. Chem.*, 2010, **49**, 6402–6408; (*b*) P.-K. Lee, W. H.-T. Law, H.-W. Liu and K. K.-W. Lo, *Inorg. Chem.*, 2011, **50**, 8570–8579; (*c*) Y. Chen, L. Qiao, L. Ji and H. Chao, *Biomaterials*, 2014, **35**, 2–13.

21 (*a*) S. Lamansky, P. Djurovich, D. Murphy, F. Abdel-Razzaq, H.-E. Lee, C. Adachi, P. E. Burrows, S. R. Forrest and M. E. Thompson, *J. Am. Chem. Soc.*, 2001, **123**, 4304–4312; (*b*) S. Lamansky, P. Djurovich, D. Murphy, F. Abdel-Razzaq, R. Kwong, I. Tsyba, M. Bortz, B. Mui, R. Bau and M. E. Thompson, *Inorg. Chem.*, 2001, **40**, 1704–1711.

22 (*a*) S. Zhang, M. Hosaka, T. Yoshihara, K. Negishi, Y. Iida, S. Tobita and T. Takeuchi, *Cancer Res.*, 2010, **70**, 4490–4498; (*b*) T. Yoshihara, Y. Karasawa, S. Zhang, M. Hosaka, T. Takeuchi, Y. Iida, K. Endo, T. Imamura and S. Tobita, in *Proc. SPIE 7190, Reporters, Markers, Dyes, Nanoparticles, and Molecular Probes for Biomedical Applications*, San Jose, CA, USA, 2009, pp. 71900X–771908.

23 J. R. Manning and H. M. Davies, *Org. Synth.*, 2007, **84**, 334–346.

24 C. Dardonville, C. Fernandez-Fernandez, S.-L. Gibbons, G. J. Ryan, N. Jagerovic, A. M. Gabilondo, J. J. Meana and L. F. Callado, *Bioorg. Med. Chem.*, 2006, **14**, 6570–6580.

25 J. V. Caspar and T. J. Meyer, *J. Am. Chem. Soc.*, 1983, **105**, 5583–5590.